Robotics and Autonomous Systems 74 (2015) 283–295

Contents lists available at ScienceDirect

Robotics and Autonomous Systems

journal homepage: www.elsevier.com/locate/robot

Enhancing the robustness of the EPSAC predictive control using a Singular Value Decomposition approach☆,☆☆

Juan A. Castano [a,*], Andres Hernandez [b,*], Zhibin Li [a], Nikos G. Tsagarakis [a], Darwin G. Caldwell [a], Robin De Keyser [b]

[a] Istituto Italiano di Tecnologia, via Morego 30, 16163 Genova, Italy
[b] Department of Electrical Energy, Systems and Automation, Ghent University, Belgium

HIGHLIGHTS

- A robust extension for MPC controllers using SVD is proposed.
- Stability and performance analysis are presented on a mass–spring–damper system.
- Closed loop characteristics are compared with the nominal implementation.
- Results show the advantages of the proposed method to enhance the robustness.
- Simulation of a Dynamic Walking of the Humanoid Robot COMAN is presented.

ARTICLE INFO

Article history:
Received 16 March 2015
Received in revised form
6 August 2015
Accepted 1 September 2015
Available online 8 September 2015

Keywords:
Model Predictive Control
Singular Values Decomposition
Biped locomotion

ABSTRACT

In this paper, we present a Robust Model Predictive Control (MPC) based on the Singular Value Decomposition (SVD) analysis to handle long prediction and control horizons where numerical instability might appear. The proposed method is developed following the Extended Prediction Self-Adaptive Control (EPSAC) algorithm. The performance of the controller is evaluated in simulation using a 4th order mass–spring–damper system, and the dynamic walking of the humanoid COMAN. The stability of the closed-loop system is analysed using root-locus and Bode plots whilst robustness tests are performed by introducing modelling errors in the prediction model. The results show that the proposed extension increases the robustness of the feedback control, and therefore the operational range of the system.

1. Introduction

Model Predictive Control (MPC) is one of the control methodologies that have been well applied in both academia and industry. Its success is due to the ability of handling nonlinear, multi-variable systems with the consideration of constraints in an efficient manner [1,2]. A number of applications of MPC have been reported in industry [3,4] as well as in research areas including fast dynamic systems such as those found in robotics [5,6].

For the MPC method, a model is needed to estimate the future behaviour of the system, where an optimization problem is solved on-line, in order to find the optimal control inputs which satisfy the constraints and minimize an objective function. As demonstrated by previous researchers, the MPC performance strongly depends on the quality of the model and the prediction of noise [7,6,8–10]. In practice, modelling errors cannot be avoided, therefore, in MPC there is a need to develop tools that ensure the closed loop stability of the system, and to define the degree of uncertainty allowed by the controller. This is important given the modelling limitations and the approximations made in the model design phase. In order to analyse the closed loop stability, three methods have been proposed in literature: root-locus analysis [2], Lyapunov analysis [11,12], and long prediction horizons based stability for MPC [13,14].

From the stability point of view, it is known that long prediction horizons can provide stability [2]. Nevertheless, this can turn into ill-defined prediction matrices [11,15]. This problem can be solved as in [2], where the optimization function is modified to provide more relevance to the short-term response, even when a long

☆ This work is supported by the FP7 European project WALK-MAN ICT-2013-10.
☆☆ This work is supported by the institute for the Promotion and Innovation by Science and Technology in Flanders IWT SBO-110006.
* Corresponding authors.
E-mail addresses: Juan.Castano@iit.it (J.A. Castano), Andres.Hernandez@UGent.be (A. Hernandez).

http://dx.doi.org/10.1016/j.robot.2015.09.001
0921-8890/

prediction horizon is used. This approach provides stability for long prediction horizons but considering only the well-conditioned problem during the optimization stage. Another way to handle this problem is to reduce the solution space by removing, from the prediction matrix, the ill-defined states of the system, with the drawback that the performance might be reduced as some dynamics are neglected.

The robustness can be enhanced in the controller by taking into account the parametric variation of the system to be controlled as in [16,17]. Another approach is to analyse how the Singular Value Decomposition (SVD) affects the system behaviour as investigated in [18], where an optimization was proposed to provide a feasible response of the system.

Following a similar trend, in our work we use the analysis and manipulation of the singular values of the optimization matrix to enhance the robustness of the MPC. In particular we use the Extended Predictive Self-Adaptive Control (EPSAC) approach to MPC [7]. The EPSAC algorithm has been chosen here because it allows the use of input/output models (e.g. transfer functions) which avoids the need of state estimators. In addition, the EPSAC algorithm is able to adapt the disturbance model, using a filter as a disturbance observer. The proposed methodology is important for the cases in which long prediction and control horizons are used. The stability of the method is analysed using the root-locus, and the robustness is validated by introducing modelling errors and parameter variations in the prediction model.

To study the properties of our improved EPSAC controller, two systems are investigated. The first example is a mass–spring–damper, which is widely used to model mechatronic systems. Its fourth order dynamics and low-damping impose a challenge for the controller. In the second example, the robust EPSAC is used to generate a smooth walking pattern of a humanoid robot by controlling the Zero Moment Point (ZMP) [19]. The implementation of the MPC controller for the latter study requires large prediction and control horizons, resulting in numerical instability of the control. The model of the humanoid COMAN[1] was simulated in the Open Dynamics Engine (ODE). In both cases, stability analysis and robustness tests are performed.

The paper is organized as follows. A brief introduction of the EPSAC algorithm is presented in Section 2. In Section 3, we motivated the use of long control and prediction horizons in MPC. In Section 4, the extension to Robust EPSAC is explained and its properties are studied. The stability is analysed by root-locus criterion in Section 5. Two case studies are presented and discussed in depth in Section 6. Finally, the main outcome of this contribution is summarized in Section 7.

2. EPSAC algorithm

MPC controllers are those that use a plant model to get the control effort that minimizes an objective function over a time horizon. The Extended Prediction Self-Adaptive (EPSAC) algorithm proposed in [7] is the MPC controller selected in this work. This controller can use different formats to represent the input/output response of the model e.g. state-space, neural networks, transfer functions, etc. In this work, the transfer function representation is used, which avoids the need to design a state estimator.

The generic process model of the EPSAC is given by

$$y(t) = x(t) + n(t), \tag{1}$$

where $y(t)$ is the measured output of the process. $x(t)$ is the modelled output, and $n(t)$ represents all the effects that are not modelled by $x(t)$ respect to $y(t)$, in a discrete time t.

[1] COmpliant huMANoid (COMAN) is developed by the Italian Institute of Technology.

$x(t)$ can be modelled with the transfer function

$$x(t) = \frac{B(q^{-1})}{A(q^{-1})}u(t), \tag{2}$$

and the disturbance $n(t)$ is filtered with transfer function

$$n(t) = \frac{C(q^{-1})}{D(q^{-1})}e(t). \tag{3}$$

To describe the non-modelled dynamics and noise, we use the filter (3) to have a coloured noise representation in a desired frequency band. $e(t)$ is uncorrelated (white) noise and A, B, C, D are monic polynomials in the backward shift operator q^{-1}. To have a better performance of the controller, the choice of (3) is designed to suit the type of disturbance [10]. However, a 'default' choice, that removes the steady-state offset is $n(t) = \frac{1}{1-q^{-1}}e(t)$ [8].

With the generic process model (1), the modelled output (2), the process disturbance model (3), and based on the superposition principle for linear systems, the predicted values of the output are

$$y(t+k|t) = y_{base}(t+k|t) + y_{opt}(t+k|t), \tag{4}$$

where

- $y_{base}(t+k|t)$ is the effect of the past inputs $u(t-1)$, $u(t-2)\ldots$, the effect of a known future control sequence $u_{base}(t+k|t)$, which can be the last used input, and the effect of disturbance $n(t+k|t)$ in the prediction horizon N_2.
- $y_{opt}(t+k|t)$ is the output due to the optimized control actions $\delta u(t|t), \ldots, \delta u(t+N_u-1|t)$, with $\delta u(t+k|t) = u(t+k|t) - u_{base}(t+k|t)$ in a control horizon N_u.

Using the discrete time convolution of the unit impulse and step responses of the system with coefficients $h_1, \ldots, h_{N_2}$ and $g_1, \ldots, g_{N_2}$ respectively, the optimized output $y_{opt}(k)$ is expressed as

$$\begin{aligned} y_{opt}(t+k|t) = {} & h_k\delta u(t|t) + h_{k-1}\delta u(t+1|t) + \cdots \\ & + g_{k-N_u+1}\delta u(t+N_u-1|t). \end{aligned} \tag{5}$$

Combining (4) and (5), and using vector notation, we have

$$\mathbf{Y} = \overline{\mathbf{Y}} + \mathbf{G}\mathbf{U}, \tag{6}$$

where

$$\begin{aligned} \mathbf{Y} &= [y(t+N_1|t)\ldots y(t+N_2|t)]^T, \\ \overline{\mathbf{Y}} &= [y_{base}(t+N_1|t)\ldots y_{base}(t+N_2|t)]^T, \\ \mathbf{U} &= [\delta u(t|t)\ldots \delta u(t+N_u-1|t)]^T, \\ \mathbf{G} &= \begin{bmatrix} h_{N_1} & h_{N_1-1} & \cdots & g_{N_1-N_u+1} \\ h_{N_1+1} & h_{N_1} & \cdots & \cdots \\ \cdots & \cdots & \cdots & \cdots \\ h_{N_2} & h_{N_2-1} & \cdots & g_{N_2-N_u+1} \end{bmatrix}, \end{aligned} \tag{7}$$

where temporal horizons N_1, N_2 and N_u are design parameters and $\mathbf{G}$ is the prediction matrix.

We find the optimal control effort $\mathbf{U}$ by minimizing the cost function below,

$$J = \sum_{k=N_1}^{N_2} [r(t+k|t) - y(t+k|t)]^2. \tag{8}$$

Notice that, as described in [7], we can use alternative cost functions other than (8). In addition, it is possible to represent the *reference trajectory* using a first-order function with initialization $r(t|t) = y(t)$ as:

$$\begin{aligned} r(t+k|t) = {} & \alpha r(t+k-1|t) + (1-\alpha)w(t+k|t), \\ & \forall k \in [1, \ldots, N_2]. \end{aligned} \tag{9}$$

The signal $w(t)$ represents the desired set-point and α is a design parameter to tune the MPC performance [3].

The compact matrix representation for the cost function (8) is

$$(\mathbf{R}-\mathbf{Y})^{\mathbf{T}}(\mathbf{R}-\mathbf{Y}) = [(\mathbf{R}-\overline{\mathbf{Y}})-\mathbf{GU}]^T[(\mathbf{R}-\overline{\mathbf{Y}})-\mathbf{GU}], \tag{10}$$

where $\mathbf{R} \in \Re^{N_2}$.

Defining

$$\begin{aligned} &\mathbf{H} = \mathbf{G}^T\mathbf{G}, \qquad \mathbf{f} = -\mathbf{G}^T(\mathbf{R}-\overline{\mathbf{Y}}), \\ &c = (\mathbf{R}-\overline{\mathbf{Y}})^T(\mathbf{R}-\overline{\mathbf{Y}}), \end{aligned} \tag{11}$$

the expression in (10) can be transformed into the standard quadratic cost index

$$J(\mathbf{U}) = \mathbf{U}^T\mathbf{H}\mathbf{U} + 2\mathbf{f}\mathbf{U} + c. \tag{12}$$

The constraints of a system should always be considered, since all processes are subject to them. Like *input constraints* for the case of limits in the actuator range, or *output constraints* for maximum output range. There are two available approaches: Clipping and Constrained Control.

Clipping approach is formulated assuming that the control effort has an unlimited range. First the control action is calculated, then it is hard-limited to keep the resulting values within the specified range. Minimizing the cost function (12) with respect to $\mathbf{U}$, leads to the optimal (unconstrained) solution $\mathbf{U}^* = -\mathbf{H}^{-1}\mathbf{f}$:

$$\mathbf{U}^* = [\mathbf{G}^T\mathbf{G}]^{-1}[\mathbf{G}^T(\mathbf{R}-\overline{\mathbf{Y}})]. \tag{13}$$

In this approach the solution obtained by (13) is limited into a minimum and maximum value, e.g. ($\min \leq \mathbf{U}^* \leq \max$).

Constrained control approach takes the constraints into account a priori, which result in an optimal solution within the specified limits, finding the solution as a constrained optimization problem, which is formulated as:

$$\begin{aligned} \min_{\mathbf{U}} \quad & J(\mathbf{U}) = \mathbf{U}^T\mathbf{H}\mathbf{U} + 2\mathbf{f}^{\mathbf{T}}\mathbf{U} + c, \\ \text{subject to} \quad & \mathbf{AU} \leq \mathbf{b}, \end{aligned} \tag{14}$$

where $\mathbf{A} \in \Re^{Nu\times(iN_u+jN_2)}$ and $\mathbf{b} \in \Re^{iN_u+jN_2}$ given i input constraints and j output constraints. The above problem is a standard quadratic programming problem.

Finally, the MPC feedback control applies only the first optimal control input $u^*(t) = u_{base}(t|t) + \delta u(t|t) = u_{base}(t|t) + \mathbf{U}^*(1)$ to the plant and then the whole procedure is repeated again at the next control sample $(t+1)$.

3. Motivation for the use of long control horizons in MPC

Literature of MPC shows that in general a control horizon $N_u = 1$ is enough to address most of the control problems [7,20], since it allows the system to follow set-point changes at its "natural" rate, while being able to react to disturbances at a rate determined by the monic polynomials C and D in (3). However, there are particular systems where a control horizon of $N_u = 1$ may result in a mean-level control that does not have an optimal performance such as the high order systems with multiple modes [21]. The use of a long control horizon provides further properties and may be required for some applications, as mentioned in [21]. Some of the properties are: a faster settling time, better tracking of a desired trajectory, and stronger noise rejection. However the system decreases its robustness and becomes more aggressive and sensitive to disturbances, this behaviour is due to the control effort, which is increased to produce a faster response.

Biped walking control is an example where long control and prediction horizons are particularly required given the necessity of an anticipated control action which takes into account the future steps of the robot in order to guarantee a good tracking performance. In our study the control target is the zero moment point (ZMP), which is the point where the ground forces acting on the body can be replaced by a single force [22]. While the ZMP remains inside the support polygon, the robot will not tip around the support polygon. The control goal is to produce a feasible COM motion that requires the ground reaction forces always from the support polygon. In other words, the ZMP is always inside the support polygon, which prevents the robot from tipping over. Given a ZMP trajectory represented by W_Z as

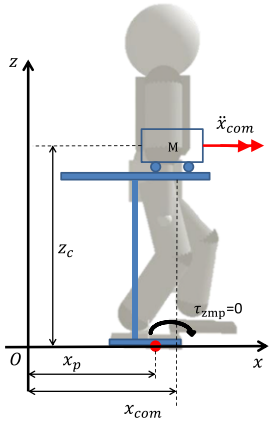

Fig. 1. The cart–table model.

$$W_Z = [w_1, w_2, \ldots, w_{N_2}], \tag{15}$$

$$\|X_{zmp} - w_1\| \leq SP_t, \tag{16}$$

where SP_t is the support polygon at time t.

In order to model the dynamics of biped walking, the cart–table model Fig. 1 proposed by [23] is used to represent the behaviour of the centre of mass (COM) of the robot. The robot is simplified as a running cart on top of a mass-less table, the cart represents the centre of mass of the robot and the table represents the supporting foot. Given the cart's acceleration, the ZMP position can be computed by

$$x_{ZMP} = x - \frac{z_c\ddot{x}}{g}, \tag{17}$$

where g is the gravity constant and z_c is the constant height of the COM. We regard ZMP as the control target, and the *jerk* (the rate of change of acceleration) as the control effort.

The control of ZMP requires an anticipated control action to guarantee a precise tracking, so the COM motion does not diverge. To realize this, the real ZMP should track the ZMP reference within the support polygon to provide a physically realizable response of the biped walking. In this case, a long prediction horizon is needed because an accurate ZMP tracking must consider future information for more than one step. By applying our proposed control strategy, we can obtain a COM trajectory that is coherent with the ZMP trajectory and with the walking strategy.

Fig. 2 shows the behaviour of the ZMP and the COM of the cart–table model when the same ZMP reference is used. The time window was 2 s and the sampling time was 5 ms corresponding to a prediction horizon of $N_2 = 400$. As it is shown, a good ZMP tracking that keeps the ZMP response close to the reference is generated when a bigger prediction horizon N_u is used. When $N_u = 1$, the system has a slower response to the changes in the reference and the settle time is longer. Each steady ZMP reference corresponds to a stationary foothold during walking, which implies that the COM should ideally transit between two successive steps.

Therefore, for the particular control requirements of the walking pattern generator, short prediction horizon does not

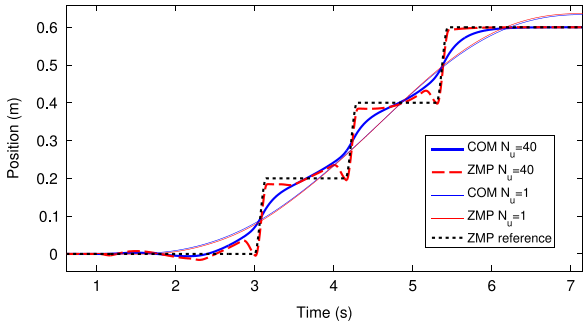

Fig. 2. Control response for short and long control horizons.

provide future information of the change of ZMP due to the discrete change of foothold, which fails to generate a dynamically stable gait. This motivates us to develop a control technique that warrants a robust response of the EPSAC controller when long prediction and control horizons are implemented, and meanwhile keep the advantages provided by the long control horizons.

4. Extension to robust EPSAC based on SVD

The EPSAC solution uses the inversion of the prediction matrix **G** (13). Consequently, the numerical stability depends on whether this matrix is well defined. The stability of the system can be extracted from the Singular Value Decomposition (SVD) [15,18], which provides also the frequency response of the system due to the control horizon and a mathematical representation of the solution space. In our work, we generate a well-defined prediction matrix for the long prediction (N_2) and control horizons (N_u). The method takes advantage of the SVD properties in order to provide robustness of the closed loop system.

Given the matrix **G** defined in (7), for $N_1 = 1$ and $h_k = 0,\ g_k = 0,\ \forall k \leq 0\,|k \in Z$, thus matrix **G** is bottom triangular with the following *economy-sized* SVD representation:

$$\mathbf{G} = \mathbf{U}\boldsymbol{\Sigma}\mathbf{V}^T, \tag{18}$$

which considers, for the computation, only the first N_u columns of U and first N_u rows of Σ.

$$\mathbf{U} = [U_1, U_2, \ldots, U_{N_2}] \in \Re^{N_2 \times N_u} \tag{19}$$

represents the left singular vectors, and

$$\mathbf{V} = [v_1, v_2, \ldots, v_{N_u}] \in \Re^{N_u \times N_u} \tag{20}$$

is the right singular vectors, and

$$\boldsymbol{\Sigma} = \mathrm{diag}[\sigma_1, \sigma_2, \ldots, \sigma_{N_u}] \in \Re^{N_u \times N_u} \tag{21}$$

is the singular values of the prediction matrix **G**. Geometrically, the SVD describes a rotated hypersphere in $\Re^{N_u}$, Fig. 3, where σ_i, for $i \in [1, 2, \ldots, N_u]$, defines the magnitudes of the space in the directions of the principal axes defined by the singular vectors [24]. If $\boldsymbol{\Sigma}$ is ill-defined, the nominal system diverges, because small changes on the singular values generate an unbounded response of the system. Conventionally, a method used to avoid this situation is to eliminate the ill-defined singular values in the representation, thus, resulting in the dimensional reduction of matrix **G**, hence, the control horizon. However, this may cause a non-desirable response because some of the inherited properties of the controller are not preserved in the new representation.

In this paper, we propose a modification of the hyperspace that keeps its dimensionality. Our method changes the magnitude of the singular values $\sigma_i\ \forall i \in k|k \leq N_u$, while the directional and rotational singular vectors remain the same. This results in a bigger hypersphere that contains the nominal solution space. The new

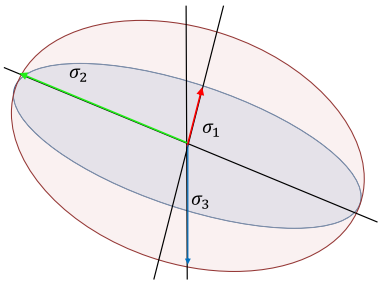

Fig. 3. Geometrical representation of the SVD.

sphere has smoother transition and higher correlation between the N_u spaces. The obtained response is more robust against the uncertainties in the model, while the complete control horizon N_u and its inherited properties are preserved during the optimization phase.

4.1. Hypersphere construction

In order to better understand the method, consider a system representation given by the parameters $\mathbf{L} = [l_1 + \delta_1, l_2 + \delta_2, \ldots, l_m + \delta_m]$ and impulse response H_L, where δ_i is the variation of the ith parameter, and let **G** be as in (7), then a SVD representation of the system is obtained with $\boldsymbol{\Sigma}_\mathbf{L} = [\sigma_{1_L}, \sigma_{2_L}, \ldots, \sigma_{Nu_L}]$. This representation maps the effect of the parameter $l_i + \delta_i$ into the SVD of the system providing the solution space to be controlled. In order to build a robust representation of the **G** matrix based on the SVD, it is possible to take the maximum σ_{i_L}, given a known variation range δ_i. This approximation covers the solution space of the system considering the worse scenario for each $\sigma_i \in \boldsymbol{\Sigma}_\mathbf{L}$. Nevertheless, we propose a fitting function based on the impulse response of the nominal system that provides a smooth transition through the hyper spaces of $\boldsymbol{\Sigma}_\mathbf{L}$, increasing the relation between the optimal control inputs $\mathbf{U}_t^*$ in the control horizon and the impulse response of the system.

We evaluate the contribution of the impulse response at the sample time $k_i > k_0$ where k_0 is the present time. The ith row of **G** contains the impulse response for $1 \leq j \leq N_u - 1$, where $G(i, j) = 0,\ \forall j > i$. Then, the relative contribution $C_p(k)$ of the impulse response h_{N_1} applied at future time $k_f = [1, 2, \ldots, N_u]$ can be expressed as

$$C_p(k) = \frac{\left|{h_{N_1}}^{\beta}\right|}{\left(\sum_{j=1}^{k} |G(k, j)|\right)^{\beta}} \times 100\%, \quad \forall k \leq N_u, \tag{22}$$

where the parameter $\beta \in \Re > 0$ is a factor that allows the method to modulate the shape of the fitting curve to guarantee that the modified singular values contain the original ones. Eq. (22) represents the percentage contribution of the impulse applied at time k_i with respect to the total contribution of impulses applied up to time k_{N_u}.

To find the k singular values of the $\boldsymbol{\Sigma}_\mathbf{C}$ where $k \in [1, 2, \ldots, Nu]$ we proceed as follows.

- For $k = 1$, $\Sigma_{C_k} = \sigma_1$ and $C_p(1) = 100\%$.
- For $k = 2, 3, \ldots, Nu - 1, Nu$ the singular values Σ_{C_k} are calculated assigning proportional weights in $C_p(k)$. These proportional weights correspond to the relative contribution of the h_{N_1} value with respect to the accumulative contribution of the impulse response.
- Reconstruct $\mathbf{G_C}$ as the new prediction matrix using (18), which is the mathematical representation of the solution space of the system dynamics.

Notice that the dimensional space is conserved since the nominal left and right singular vectors are constant. This implies that the growing direction and the rotational space of the original solution are consistent with the new representation.

4.2. Robustness analysis

Consider $\mathbf{G} \in \Re^{N_2 \times N_u}$, the optimization that provides the control effort at present time t is obtained by a minimization process influenced by the future inputs up to time $t + N_u$. From the SVD, the effect of the input at time $t + i$, for $i = 1, 2, \ldots, N_u$, is directly related to the corresponding value $\sigma_i \in \mathbf{\Sigma}$. To guarantee a robust response of the closed loop system, the hyperspace described by $\mathbf{\Sigma_C}$ must contain the nominal space solution. The proposed method constructs the hyperspace that contains the nominal one using (22) and the maximum singular value of the nominal system. If the singular values of the modified $\mathbf{G}$ matrix are smaller than those in the nominal representation. Then, the nominal solution space will not be contained in the new space, which reduces the system performance and its robustness. For such scenarios, a smaller β can be used, providing smoother transitions of the singular values.

The control effort will be optimized using the modified matrix $\mathbf{G_C}$, however, the prediction depends on the nominal model. Hence, a mismatch between $\mathbf{G_C}$ and the model of the system may cause a violation of the constraints. Therefore, soft constraints should be implemented to guarantee a feasible solution during the optimization. Other solution to this problem is given in [2], where the cost function was modified using weights during the optimization for each of the components in the control horizon. Their method reduces the contribution of the further components of the resulting vector, thus also reducing the effect introduced by the long control horizon. For well-defined matrices, our proposed method slightly affects the original SVD representation, i.e., the original space and the approximated solution are consistent as shown in [25].

5. Stability analysis

In the state of the art of MPC, there are different methods to prove the stability of the closed loop system. A recent stability approach for MPC controllers has been introduced. The methodology uses the intrinsic stability of long prediction horizon MPC controllers [2,13,26]. However, in this work, we focus on the root-locus representation as reported in [2], which is a classical scheme to verify the stability given the poles distribution.

As presented in [2], for the unconstrained control problems, we can obtain a root locus representation of the closed loop system as follows:

$$\mathbf{U}^* = [\mathbf{\Phi^T \Phi}]^{-1}[\mathbf{\Phi^T}(\mathbf{R} - \mathbf{Fx(k)})], \tag{23}$$

where $x(k)$ are the states of the system at time k and $\mathbf{F} = [\mathbf{CA\ CA^2} \ldots \mathbf{CA^{N_2}}]^{\mathbf{T}}$. The solution (23) is consistent with (13), thus we conclude that $\Phi \equiv \mathbf{G}$ and $Fx(k) \equiv \overline{Y}$.

From the analytical solution (23) and (13), we observe that the term

$$[\mathbf{G}^T\mathbf{G}]^{-1}\mathbf{G}^T\mathbf{R} \tag{24}$$

corresponds to the set point change, while the term

$$-[\mathbf{G}^T\mathbf{G}]^{-1}\mathbf{G}^T\mathbf{F} \tag{25}$$

corresponds to the state feedback control within the framework of predictive control. Both terms depend on the system parameters, and are constant matrices for a time-invariant system. Based on the receding horizon, only the first value of U^* is applied, yields:

$$\mathbf{U}^* = K_y\mathbf{R}(k) - \mathbf{K_{MPC}}\mathbf{x}(k), \tag{26}$$

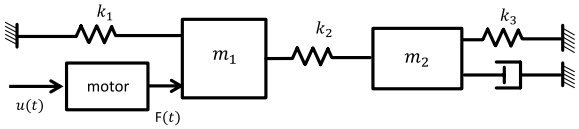

Fig. 4. Schematic representation of the mass–spring–damper system.

where K_y is the first element of the matrix $[\mathbf{G}^T\mathbf{G}]^{-1}\mathbf{G}^T\mathbf{R}$ and $\mathbf{K_{MPC}}$ corresponds to the first row of $[\mathbf{G}^T\mathbf{G}]^{-1}\mathbf{G}^T\mathbf{F}$. The standard state feedback law can be represented as

$$\begin{aligned}\mathbf{x}(k+1) &= \mathbf{Ax}(k) - \mathbf{BK_{MPC}}\mathbf{x}(k) + \mathbf{B}K_y\mathbf{R}(k)\\ &= (\mathbf{A} - \mathbf{BK_{MPC}})\mathbf{x}(k) + \mathbf{B}K_y\mathbf{R}(k).\end{aligned} \tag{27}$$

Thus, the closed loop eigenvalues can be evaluated through the characteristic equation:

$$\det[\lambda\mathbf{I} - (\mathbf{A} - \mathbf{BK_{MPC}})] = 0. \tag{28}$$

6. Simulation results

In order to evaluate the performance of the proposed strategy, two systems are studied: a mass–spring–damper system and the dynamic walk of a humanoid robot. The description of the two systems and the main results obtained are discussed in the following subsections.

6.1. Mechatronic system: mass–spring–damper

In this example, we apply the proposed technique to a mass–spring–damper system as in Fig. 4. The input of the system is the voltage applied on the motor $u(t)$ and the outputs are the mass displacements $y_1(t)$ and $y_2(t)$. Therefore, a complete model of the electromechanical plant should represent the dynamics from $u(t)$ to $y_1(t)$ and from $u(t)$ to $y_2(t)$. The electrical dynamics of the motor is much faster than the mechanical dynamics thus can be neglected, and the motor can be represented by a pure static gain $F(t) = Ku(t)$, with $F(t)$ the force on the 1st mass. The parameters of the set-up are: $m_1 = 1.85$ kg, $m_2 = 1.35$ kg, $k_1 = k_2 = 800$ N/m, $k_3 = 450$ N/m, and $c_1 = 9$ N/(m/s).

The transfer function of the control response from the motor to the second mass m_2 is

$$\Gamma(s) = \frac{Y_2(s)}{U(s)} = \frac{k_2}{\Psi}, \tag{29}$$

where

$$\begin{aligned}\Psi &= m_1m_2s^4 + m_1c_1s^3 + m_1s^2(k_2 + k_3)\\ &\quad + m_2s^2(k_2 + k_1) + c_1s(k_2 + k_1) + k_2k_3 + k_1k_2 + k_1k_3.\end{aligned}$$

Applying the numerical values to (29), we obtain:

$$\Gamma(s) = \frac{800}{2.498s^4 + 16.65s^3 + 4473s^2 + 14\,400s + 1\,360\,000}. \tag{30}$$

Then, we proceed with the implementation of the nominal and Robust EPSAC controller with parameters $N_1 = 1, N_2 = 30, N_u = 4$ and different β values as $\beta = 0.2$, $\beta = 0.4$ and $\beta = 0.6$ for the case study.

Fig. 5 shows that the response of the system does not have any overshoot and the required control effort is high when the EPSAC implementation is used. Additionally, it is analysed the response of the system for the robust implementation when different values of β are used. For $\beta = 0.2$, the system produces a smooth response with a small control effort. However, it presents steady-state error. For the case of $\beta = 0.4$ the response is similar to the nominal controller in terms of overshoot and settling time, but requiring

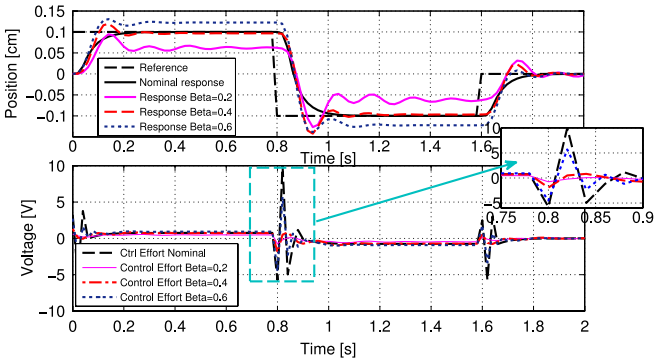

Fig. 5. System and control effort responses for different controllers.

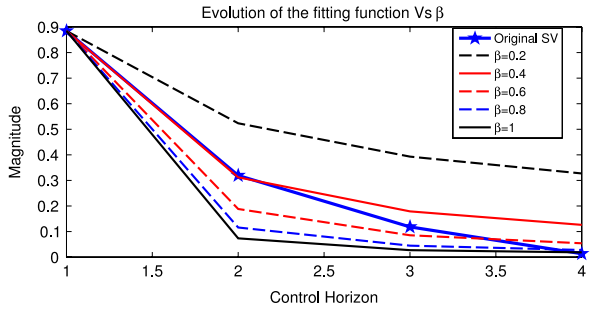

Fig. 6. Singular values for the robust EPSAC for different values of β, Solution space.

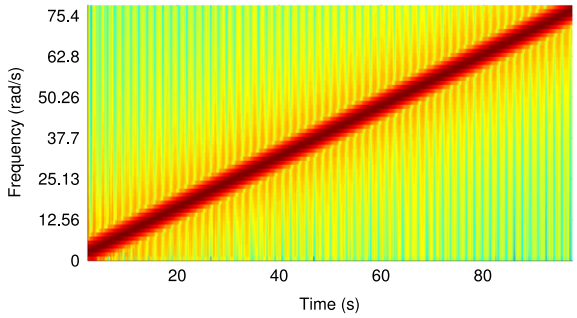

(a) Frequency spectrum of the chirp signal used for closed-loop identification.

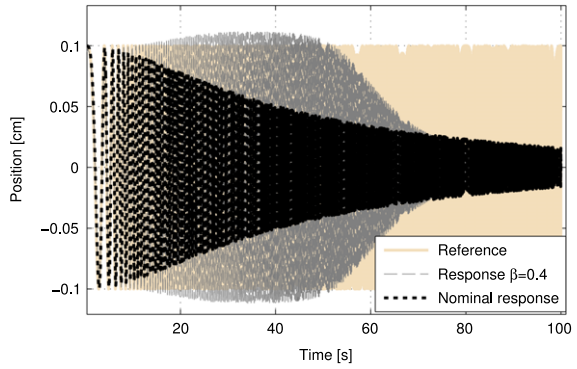

(b) Time response of the identification signal.

Fig. 7. Frequency spectrum and Time response of signal used for closed-loop identification.

a lower control effort. Finally, the case of $\beta = 0.6$ presents the lowest performance, presenting steady-state error and a control effort comparable to the nominal controller.

Given the response of the different controllers, the robust implementation when $\beta = 0.4$ is the one that reaches the best performance. This implementation leads to a response without steady state error and the overshoot of the output has comparable magnitude compared with the ones obtained from $\beta = 0.2$ and $\beta = 0.6$. Additionally, the generated control effort is lower compared to the nominal and $\beta = 0.6$ cases, but slightly higher compared to the one when $\beta = 0.2$. Finally the settling time is the same as the ones from the nominal case and the other robust implementation.

As preliminary conclusion we observe that the β parameter strongly influences the closed loop response, producing a stable response but with steady state error. This characteristic is due to the differences associated with the solution space. When β is bigger, the singular values are smaller than the nominal ones and the response is more aggressive. On the contrary, when a lower β is used, the response becomes smoother.

The magnitude of the solution space related to the SVD for different β values is depicted in Fig. 6. When the SVD is applied to the system using $\beta = 0.4$, the resulting representation is almost equal in the first two singular values compared to the nominal SVD. The further singular values, associated to the additional states of the control horizon N_u, are bigger than those in the nominal SVD, providing a more robust response of the system.

We also study the closed-loop frequency response through Bode analysis. For this aim, we apply a reference signal such that it makes a swap from $t = 0$ s with frequency $\omega = 0$ rad/s to $t = 100$ s with frequency $\omega = 78.5$ rad/s (12.5 Hz) with a spectrum as present in Fig. 7(a). The time responses for the nominal controller and the robust controller when using $\beta = 0.4$ are shown in Fig. 7(b). It is seen that the nominal time response has a low cut-off frequency, while the robust controller has a flat response up to the cut-off frequency at $t = 50$ s that corresponds to a frequency of $\omega \approx 40$ rad/s if we compare to Fig. 7(a). Using these data, we reconstruct the closed-loop transfer function of the system and analyse the frequency response using Bode plots.

As shown in Fig. 8, the nominal frequency response does not have overshoot, the magnitude stability margin is in a higher frequency compared with the other controllers being at $\omega = 51$ rad/s. However, the phase margin is in $\omega = 4.9$ rad/s being located in a smaller frequency than the robust implementations. The frequency response of the robust controller when $\beta = 0.2$ has negative steady state error in low frequencies and two overshoots in $\omega = 23$ rad/s and $\omega = 39$ rad/s. A similar response is obtained from the robust controller when $\beta = 0.4$ which presents a low steady state error and an overshoot located in $\omega = 23$ rad/s. This overshoot is similar in magnitude to the one when $\beta = 0.2$. The closed-loop response when $\beta = 0.6$ has positive steady state error but no overshoot. These qualitative analyses are better seen in Fig. 9 where we present a zoomed view of the magnitude Bode plot.

The numerical results of the closed-loop response are presented in Table 1, where we summarize the Steady State Error (SSE), the Gain Margin (GM), Phase Margin (PM) and overshoot percent (OS%). The nominal controller has the lowest frequency for the phase stability margin. The robust implementation with $\beta = 0.4$ presents the lowest SSE of the robust implementations. The stability margins for the different robust controllers are close to each other and have higher frequency than the phase margin of the nominal case. Near to the cut-off frequency, the controller produces an overshoot of magnitude 1.52 db [23.9 rad/s] that is smaller to the SSE when $\beta = 0.6$ and almost equal to the second overshoot when $\beta = 0.2$ (1.54 db [38.9 rad/s]). From the frequency analysis, we can conclude that the best performance is achieved by the robust implementation when $\beta = 0.4$. This implementation has stability margins in higher frequencies compared to the phase margin of the nominal case, and are close to the stability margins in other robust implementations. Additionally, $\beta = 0.4$ control has the smallest steady state error of

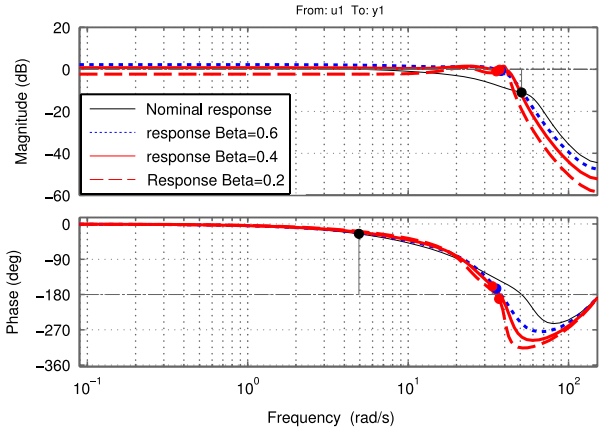

Fig. 8. Closed-loop frequency response for different controllers.

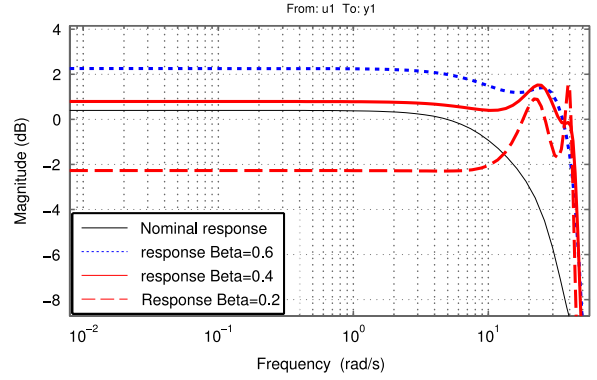

Fig. 9. Zoomed magnitude closed-loop frequency response for different controllers.

Table 1
Close loop frequency response comparison.

Controller	Parameter	Value
Nominal	SSE	0.39 db [4.5%]
	GM	11 db [51 rad/s]
	PM	155° [4.9 rad/s]
	OS	NA,
$\beta = 0.2$	SSE	−2.26 db [−22.9%]
	GM	1 db [35.5 rad/s]
	PM	−11.4° [37 rad/s]
	OS	10% [23.1 rad/s], 19.4% [38.9 rad/s]
$\beta = 0.4$	SSE	0.79 db [9.5%]
	GM	0.186 db [37.2 rad/s]
	PM	21.2° [33.5 rad/s]
	OS	19.1% [23.1 rad/s],
$\beta = 0.6$	SSE	2.25 db [29.5%]
	GM	0.755 db [37.9 rad/s]
	PM	15.3° [35.5 rad/s]
	OS	NA

the robust implementations, and the overshoots in the frequency spectrum have similar magnitudes compared to those when $\beta = 0.2$.

Considering the previous analysis, from now on, we compare the performance of the method using the nominal controller and the robust representation with $\beta = 0.4$. Fig. 10 shows the pole distribution of the closed loop system. It can be seen that the pole distribution for the robust representation ($\star$) indicates a damped behaviour and the poles are located on the right hand side, which minimizes the control effort oscillation known as ringing effect. For the EPSAC controller, the poles are located in the real axis

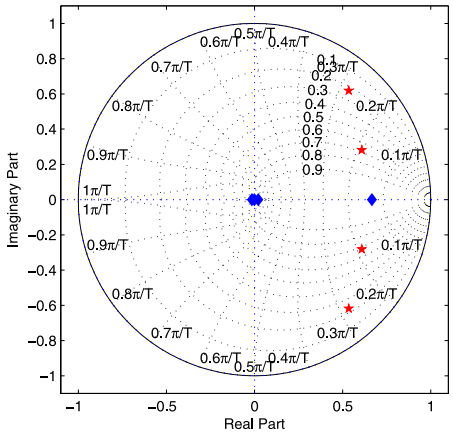

Fig. 10. Root locus representation for EPSAC and robust EPSAC controllers.

Table 2
Parametric variation for the parameter k_2.

Controller	$k_2^{\min}$ N/m	$k_2^{\max}$ N/m
EPSAC	650	850
Robust EPSAC	700	950

Table 3
Parametric variation for the parameter m_1.

Controller	$m_1^{\min}$ (kg)	$m_1^{\max}$ (kg)
EPSAC	1.73	2.25
Robust EPSAC	1.55	2.1

which means that the system is not damped as the one in Fig. 5. However, some of the poles are located on the left hand side, which generates high frequency behaviours in the control effort, which is not desired even if the stability of the system is not compromised.

To study the robustness of the controllers, we compare the responses of the system for different variations of the parameters m_1 and k_2 in (29). The parameter k_2 directly affects the gain of the system while m_2 increases the damping behaviour due to the pole distribution. For each controller, the parameters of the plant are changed from the minimum to the maximum values. This procedure is carried out until an acceptable closed loop performance is obtained. The ranges are presented in Tables 2 and 3.

First, the results obtained after introducing variations in k_2 are analysed, i.e. we consider modelling errors in the parameter k_2. As shown in Fig. 11, when the minimum value for the EPSAC controller ($k_2 = 650$) is used, the robust EPSAC performance decreases the system's performance. The settling time of the system is longer, and the response has oscillations but is still stable. For other variations of k_2, the system converges to the desired reference with a similar behaviour compared to the nominal case in Fig. 5. On the other hand, if we perform the same simulation using the nominal EPSAC controller, Fig. 12, the response is similar to the previously described one in the robust case for $k_2 = 650$. However, once the maximum k_2 is used, defined as limit for the Robust EPSAC, the system oscillates.

A similar procedure, with variations on the parameter m_1 as listed in Table 3 was implemented. Results show that the proposed robust controller outperforms the nominal EPSAC controller in terms of robustness, as the controller is stable for wider variations of m_1.

Fig. 13 shows that the robust controller performs in a wider error uncertainty in the model parameter m_1 Table 3. The nominal EPSAC has a more stable response within the selected range for the nominal case. However, if we apply $m_1 = 1.55$ kg that

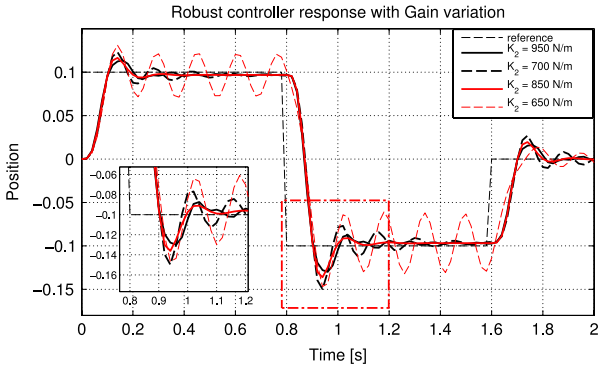

Fig. 11. System responses for the Robust EPSAC with model errors in the parameter k_2.

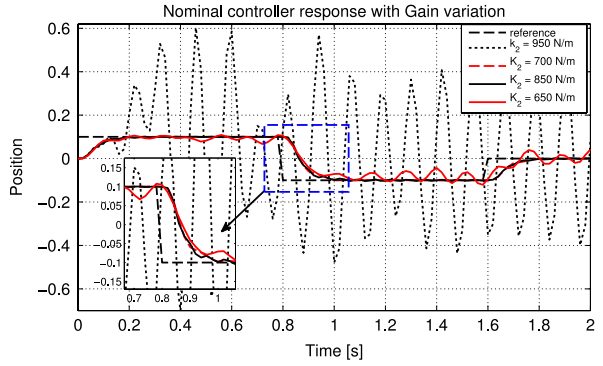

Fig. 12. System responses for the nominal EPSAC with model errors in the parameter k_2.

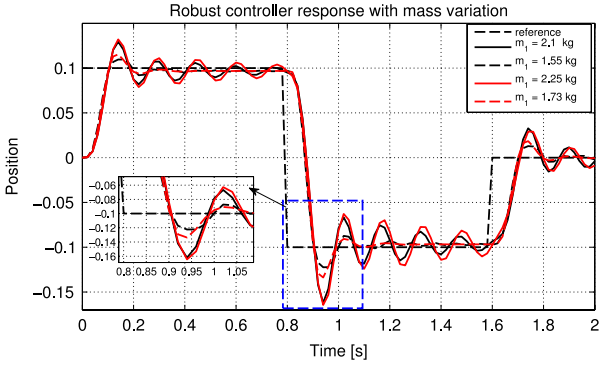

Fig. 13. System responses for the Robust EPSAC with model errors in the parameter m_1.

is the minimum value selected for the robust controller, the closed loop system with the nominal EPSAC controller oscillates as shown in Fig. 14. According to the simulated results, the robust implementation of the EPSAC controller provides a stable controller for a wider range of parameter errors while the control effort is lower as previously shown in Fig. 5, providing significant advantages.

An additional and interesting evaluation is the behaviour of the system against external disturbances applied at the input and the output of the process. In this example, we evaluate the performance of the system at a frequency of 20 rad/s, which was selected according to the frequency response of the system.

Fig. 15 shows the Bode diagram of the open loop system where the location of the resonance frequencies is located at 20 rad/s and 37 rad/s. The first frequency is studied in this work. For the noise rejection study at the input of the plant, a white noise signal with amplitude of 1 V peak-to-peak was generated. This signal

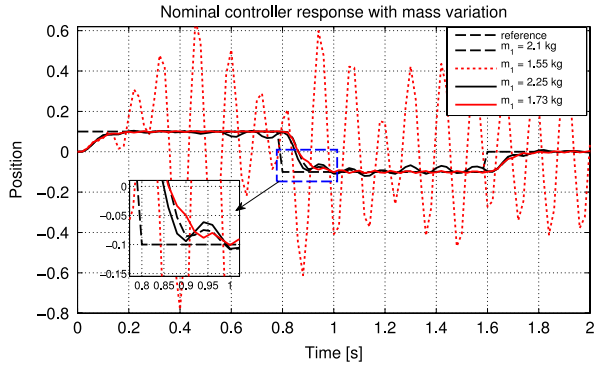

Fig. 14. System responses for the EPSAC with model errors in the parameter m_1.

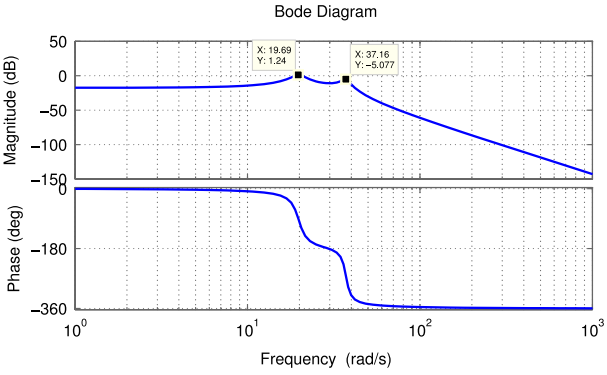

Fig. 15. Bode plot of the process.

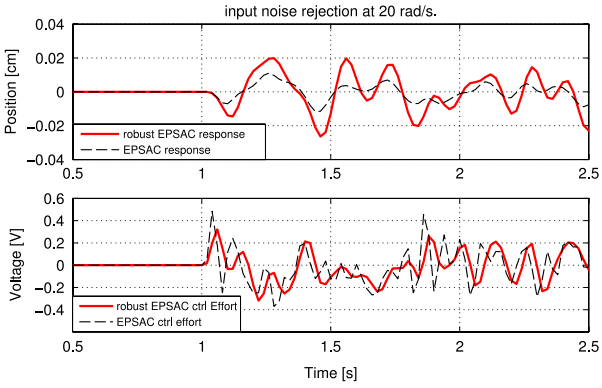

Fig. 16. System response against an input noise with $\omega = 20$ rad/s and 1 V amplitude.

was filtered using a second order Butterworth filter with cut-off frequency at 20 rad/s. The reference was constantly at zero.

As shown in Fig. 16, both controllers are able to compensate for the noise input with a similar control effort. The proposed controller has a bigger output error than the nominal controller. However given the error ranges, it can be seen that both controllers are feasible from the implementation and performance point of view.

Next, the output disturbance rejection analysis of the closed loop system is studied. In this case, the noise signal has amplitude of ± 5 mm and two frequencies are studied: 5 rad/s and 20 rad/s. This noise signal is added to the position feedback measurement.

For the measurement noise at 5 rad/s is shown in Fig. 17, both controllers reject the disturbance. The nominal EPSAC controller produces some peaks at time 3 s and has higher control effort compared to our proposed robust implementation. It shall be noted that the proposed robust EPSAC requires a lower control effort while warranting a consistent noise rejection.

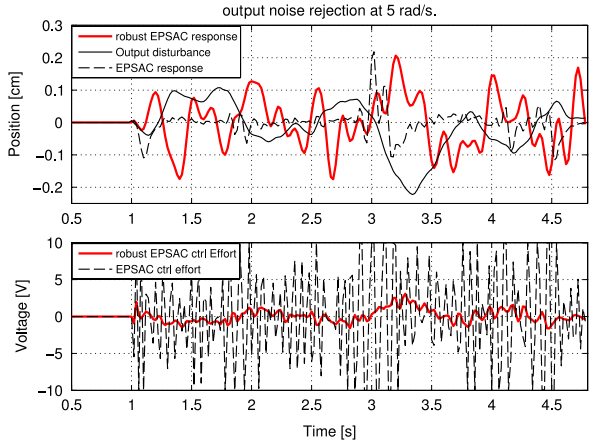

Fig. 17. System response against an output disturbance of $\omega = 5$ rad/s and ± 5 mm amplitude.

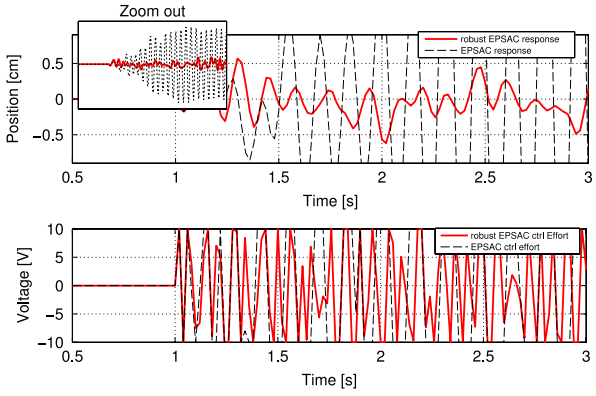

Fig. 18. System response against an output disturbance of $\omega = 20$ rad/s and ± 5 mm amplitude.

It is shown in Fig. 18 that the nominal controller is not able to reject the feedback noise thus the system oscillates. Instead, our robust EPSAC controller is able to deal with the disturbance with an amplitude error of 5 mm which is coherent with the noise magnitude. Notice that in this case only the robust controller provides a stable response.

As it was shown in the un-biased simulation study, the Robust implementation of the EPSAC controller provides significant advantages to the system's response including the robustness against modelling errors while a good control performance is obtained at the same time. Simulation studies show that the control effort is reduced while a more damped and less aggressive response is produced. Additionally, good rejection for input and output noise disturbances in a wider range is achieved by using our proposed technique.

6.2. Dynamic walking of humanoid robot COMAN

As introduced before, bipedal walking imposes the control challenge where long prediction and control horizons are required, particularly for online modulated reactive walking gaits. In this example, we show the implementation of the Robust EPSAC controller on a reactive walking gait on the humanoid COMAN. Different works have used predictive control techniques in order to produce a stable walk [27–29], among others. However, as presented in [25] for our reactive walking gait, the nominal controller EPSAC is not feasible for implementation once the reactive ZMP trajectory is used. The proposed walking strategy has an online

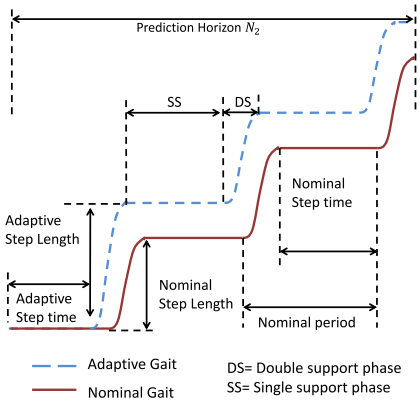

Fig. 19. Reactive ZMP gait.

ZMP trajectory generator that updates the ZMP robot's trajectory at every control loop using the feedback from the robot.

In our framework, the ZMP reference is regenerated online as in Fig. 19. The nominal gait represents a fixed and predefined ZMP trajectory, where the double support and single support phases are already known. However, the reactive gait modulates the foothold given by the foot placement and landing time predictions [25]. The new ZMP trajectory is modified based on the duration of the current single support phase and the future double support phase, depending on the current COM states and the predicted final COM states. The feet trajectories are designed coherently with the reactive gait. More details can be found in [25], and we keep the description of the reactive gait generation out of the scope in this paper.

To generate a feasible gait, the required ZMP must be restricted within the support polygon formed by the physical contacts [30] so the robot keeps the stability during the gait. Given that the system is non minimum phase, instantaneous updates of the ZMP reference in the prediction horizon produces an undershoot on the system's response. To overcome this problem, acceleration constraints must be considered [25,31].

Since the real ZMP response should track the ZMP reference within the support polygon, the ZMP x_p should match a constraint such that

$$x_{foot} - \Delta_x^- \leq \bar{x}_p \leq x_{foot} + \Delta_x^+, \tag{31}$$

where Δ_x^+, Δ_x^- is defined according to the size of the support polygon. The operator $\bar{(\cdot)}$ indicates the saturated state of the variable. These ZMP constraints, due to the support polygon, can be rewritten as acceleration constraints

$$\bar{\ddot{x}} = \begin{cases} \ddot{x}_{\min} = \dfrac{x - (x_{foot} + \Delta_x^+)}{z_c} g, \\ \ddot{x}_{\max} = \dfrac{x - (x_{foot} - \Delta_x^-)}{z_c} g. \end{cases} \tag{32}$$

In Fig. 20, the ZMP reference and the COM feedback coming from the biped, are used in the Robust EPSAC controller to generate the *jerk* (rate change of the acceleration) as the control effort to minimize the error. The generated control effort u is then constrained to generate $\bar{u}$ so that the ZMP remains within the stability region. The saturated control effort is then evaluated in the cart–table model, generating the centre of mass reference to be followed during the next control loop. This reference is mapped to the joints level by the inverse kinematics of the robot.

To implement the EPSAC control in the cart table model (Fig. 1), we use a constant height $z_c = 0.41$ m. The space state representation of the system is,

$$\dot{\mathbf{x}} = \mathbf{A}\mathbf{x} + \mathbf{B}U$$

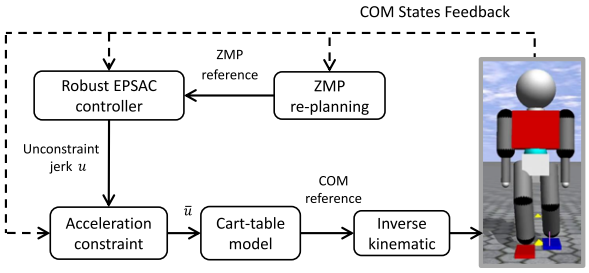

Fig. 20. Closed loop system representation.

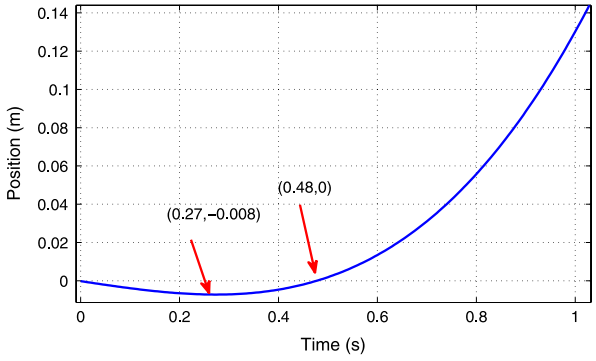

Fig. 21. Cart table model step response. $z_c = 0.41$ m.

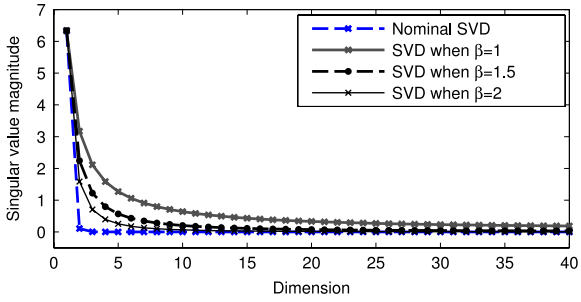

Fig. 22. SVD for the cart–table model $N_u = 40$.

$$y = \mathbf{C}\mathbf{x} + \mathbf{D}U$$

$$\mathbf{A} = \begin{bmatrix} 0 & 1 & 0 \\ 0 & 0 & 1 \\ 0 & 0 & 0 \end{bmatrix} \qquad \mathbf{B} = \begin{bmatrix} 0 \\ 0 \\ 1 \end{bmatrix}$$

$$\mathbf{C} = \begin{bmatrix} 1 & 0 & -z_c/g \end{bmatrix} \qquad \mathbf{D} = [0], \tag{33}$$

for the prediction model in the Robust EPSAC controller (2), we used the transfer function representation, substituting $z_c = 0.41$, the transfer function is:

$$\Gamma(s) = \frac{0.041794(s - 4.892)(s + 4.892)}{s^3}. \tag{34}$$

The step response is shown in Fig. 21 where the non-minimum phase duration of 0.475 s is observed.

In Fig. 22, the singular values for the Nominal EPSAC and different robust EPSAC implementations are presented. For the desired control horizon, the modified dimensional space contains the solution space of the original system when $\beta = 1$. If different β are used, some of the dimensional spaces generate an ill-defined representation. Using $\beta = 1$ provides us the properties of the long prediction and control horizons as well as those of the proposed method including the numerical stability and a better disturbance rejection.

The proposed ZMP constraint (32) was used, and a modelled error in the parameter z_c introduced into the estimation model for

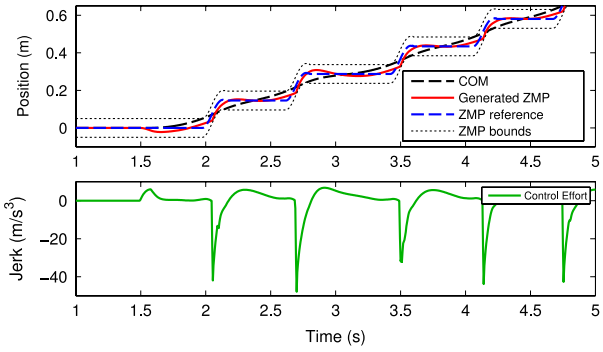

Fig. 23. Robust ZMP responses when $z_c = 0.38$ m.

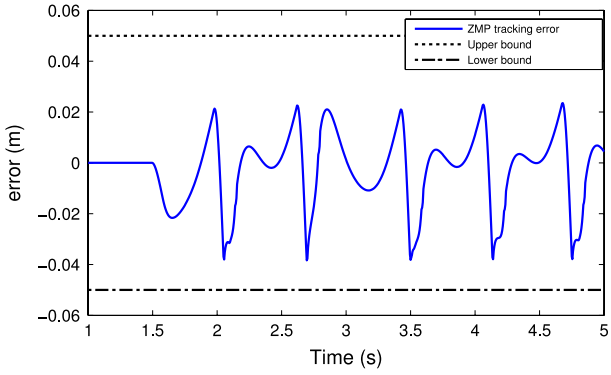

Fig. 24. Robust ZMP error responses when $z_c = 0.38$ m.

the performance analysis. The height, z_c, of the cart–table model that represents the real system was fixed to $z_c = 0.41$ m while in the prediction model for the Robust EPSAC the variable was set as $z_c = 0.38$ m. Therefore, the controller should guarantee stable trajectories with a COM height modelling error. The desired gait trajectories were built with an online generator as the introduced one.

When we apply the Robust EPSAC, the response of the closed loop system is stable as shown in Fig. 23. The ZMP trajectory is soft and continuous because of the adaptive reference and the control effort is soft. These results are consistent with those previously presented.

In Fig. 24, the errors for the constrained case are presented. The constrained response remains inside the desired bounds (± 0.05 m) throughout the motion. Notice that the foot size of the humanoid COMAN is 20 cm so the ZMP trajectory can be performed and the constrained error will not affect the feasibility in a further implementation.

As a comparison, if we apply the robust control strategy with $\beta = 1.5$, the response of the system is shown in Fig. 25, where the generated ZMP response is also feasible and the output has no oscillations. However, the simulated control effort has bigger magnitude compared to the one presented in Fig. 23 and higher frequency component.

6.2.1. Whole body humanoid simulation results

Finally, simulations on the 3*D* model of humanoid COMAN were performed. The COMAN robot is a whole body humanoid with 25 Degrees Of Freedom (DOF): 13 in the upper body, including neck, elbow, shoulders and waist and 6 DOF in each leg. The weight distribution and dimensions for COMAN are detailed in [32].

To generate the reactive ZMP trajectory, the COM states are used as feedback, and the control strategy described in Fig. 20 is used. The feet trajectories are consistently re-planned according

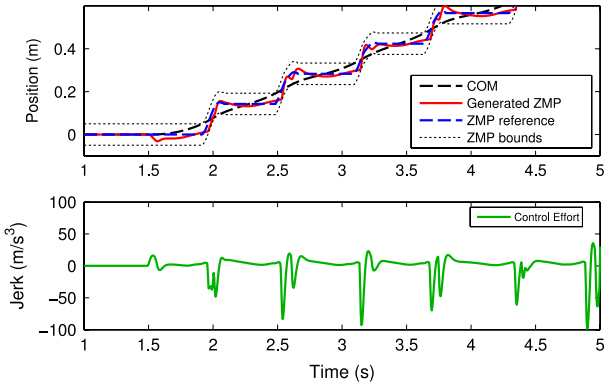

Fig. 25. ZMP responses when $z_c = 0.38$ m and $\beta = 1.5$.

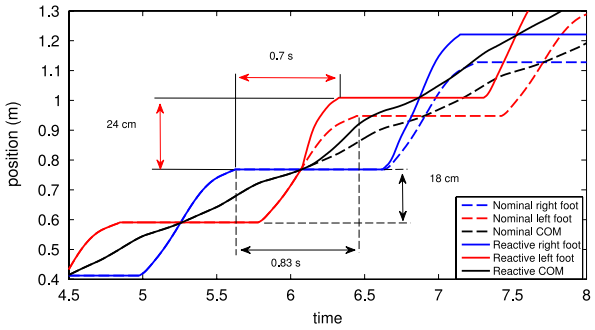

Fig. 27. Simulation data of COM and feet trajectory responses of COMAN.

to the ZMP reference, as presented in [25]. The process runs at a sampling time of 5 ms.

The Robust EPSAC controller tracks the re-planned ZMP reference considering the acceleration constraints and generates an adaptive COM motion. The joint trajectories of the biped are obtained by inverse kinematics given the COM and feet trajectories. The selected gait parameters are: step length $S_L = 0.2$ m, step time $S_T = 0.8$ s, constant COM height $z_c = 0.38$ m and sampling time $T_s = 5$ ms. The desired COM trajectory is adapted to the changes on the robot's COM states while the ZMP is contained into the stability region using (32).

A disturbance was created by a flying ball that hit the back of the robot at a horizontal speed of 6 m/s and a mass of 2 kg, the response of the biped is presented in Fig. 27. The step length was adjusted by 6 cm in order to counterbalance the disturbance and maintain a stable gait by modifying the ZMP trajectory. As it is shown, the COM trajectory generated by the Robust EPSAC allowed the robot to perform such motion and compensate for the disturbance to recover balance.

Fig. 26 shows snapshots of how the robot performs a reactive walking gait when an external disturbance was applied, the proposed strategy allows the humanoid COMAN to perform a stable walking gait with a reactive ZMP generator. The closed loop system's response rejects external disturbances and keeps the stability of the robot while walking on flat terrain. Additionally, it generates a smooth COM trajectory even when fast changes in the ZMP trajectory are applied within the prediction window, providing a feasible solution for biped locomotion.

7. Conclusions

In our presented work, an extension to MPC has been proposed to enhance the robustness of the closed loop response. The method uses the Singular Values Decomposition representation of the optimization matrix, for dealing with numerical instability when long control horizons are needed.

Simulation studies on two challenging validations from the control point of view are presented: a 4th order mass–spring–damper system and the dynamic walking of a humanoid. The results show the feasibility of the proposed methodology and the improvement on the controller robustness, where stability analysis was also performed by means of root-locus and Bode plots analysis.

Promising results were obtained with the mass–spring–damper system from which we concluded that even for a well-defined system, the methodology allows to enhance the closed loop robustness. Of particular interest are the results obtained for dynamic walking of the biped robot, because in order to achieve the desired closed loop performance, it is required to design

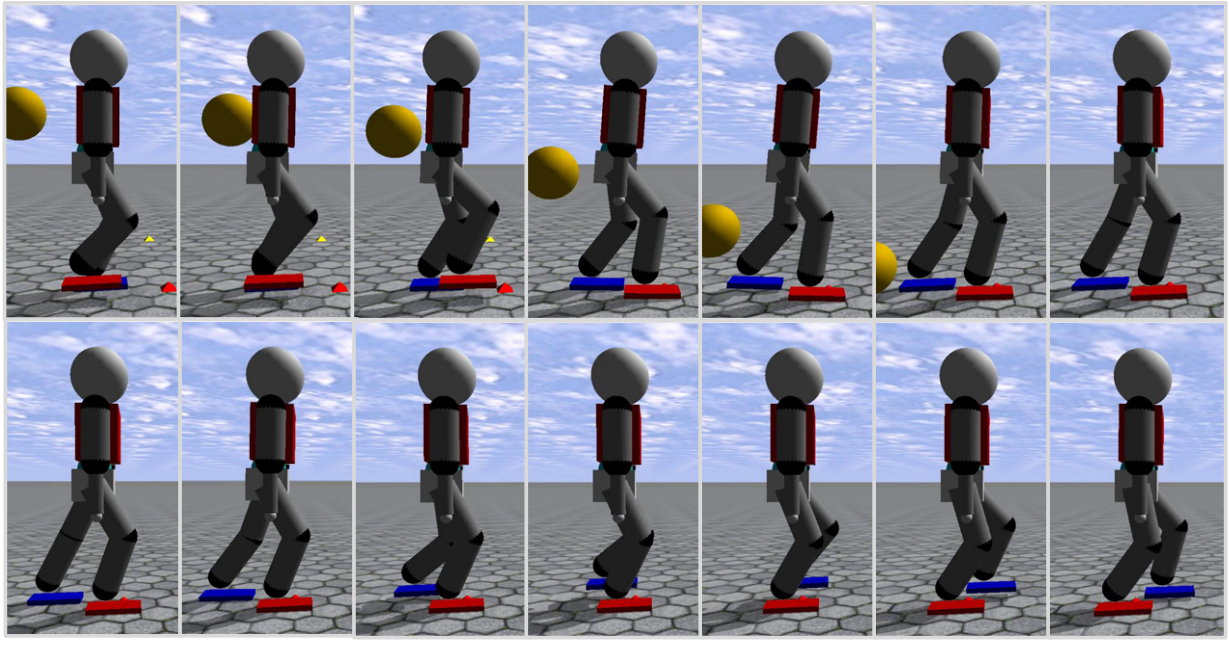

Fig. 26. Snapshots of reactive and dynamic walking in the ODE simulation.

the controller with long prediction and control horizons, causing numerical instability. The proposed robust EPSAC demonstrated robustness and smoothly tracks a walking pattern even with modelling errors.

We conclude that the proposed methodology based on SVD is suited for systems that require large prediction and control horizons to improve the robustness of the response. Future work includes the validation of the simulation results on the real platforms and the extension of the method for different systems.

References

[1] E.F. Camacho, C. Bordons, ModeL Predictive Control, second ed., Springer-Verlag, London, ISBN: 1-85233-694-3, 2004.

[2] L. Wang, Model Predictive Control System Design and Implementation Using MATLAB®, in: Advances in Industrial Control, Springer, ISBN: 9781849968362, 2010.

[3] J. Sánchez, J. Rodellar, Adaptive Predictive Control: From the Concepts to Plant Optimization, in: Prentice-Hall International Series in Systems and Control Engineering, Prentice Hall PTR, ISBN: 9780135148617, 1996.

[4] Badgwell Qin, A survey of industrial model predictive control technology, Control Eng. Pract. 11 (2003) 733–764.

[5] P.B. Wieber, Trajectory free linear model predictive control for stable walking in the presence of strong perturbations, in: International Conference on Humanoid Robots, 6th IEEE-RAS, 2006, pp. 137–142.

[6] M. Parsa, M. Farrokhi, Robust nonlinear model predictive trajectory free control of biped robots based on nonlinear disturbance observer, in: 18th Iranian Conference on, Electrical Engineering, ICEE, 2010, pp. 617–622.

[7] R. De Keyser, Model Based Predictive Control for Linear Systems, in: UNESCO Encyclopaedia of Life Support Systems, Eolss Publishers Co. Ltd., Oxford, 2003, p. 35. Article contribution 6.43.16.1 (available online at: http://www.eolss.net/sample-chapters/c18/e6-43-16-01.pdf).

[8] J. Maciejowski, Predictive Control: With Constraints, in: Pearson Education, Prentice Hall, ISBN: 9780201398236, 2002.

[9] S. Kanev, M. Verhaegen, Robustly asymptotically stable finite-horizon MPC, Automatica (ISSN: 0005-1098) 42 (12) (2006) 2189–2194.

[10] R. De Keyser, C. Ionescu, The disturbance model in model based predictive control, in: Proceedings of 2003 IEEE Conference on Control Applications. CCA. vol. 1, 2003, pp. 446–451.

[11] J. Rawlings, K. Muske, The stability of constrained receding horizon control, IEEE Trans. Automat. Control (ISSN: 0018-9286) 38 (10) (1993) 1512–1516. http://dx.doi.org/10.1109/9.241565.

[12] A. Jadbabaie, J. Hauser, On the stability of receding horizon control with a general terminal cost, IEEE Trans. Automat. Control (ISSN: 0018-9286) 50 (5) (2005) 674–678. http://dx.doi.org/10.1109/TAC.2005.846597.

[13] G. Grimm, M. Messina, S. Tuna, A. Teel, Model predictive control: for want of a local control Lyapunov function, all is not lost, IEEE Trans. Automat. Control (ISSN: 0018-9286) 50 (5) (2005) 546–558. http://dx.doi.org/10.1109/TAC.2005.847055.

[14] M. Alamir, G. Bornard, Stability of a truncated infinite constrained receding horizon scheme: the general discrete nonlinear case, Automatica (ISSN: 0005-1098) 31 (9) (1995) 1353–1356. http://dx.doi.org/10.1016/0005-1098(95)00042-U.

[15] O. Rojas, G. Goodwin, On the asymptotic properties of the Hessian in discrete-time linear quadratic control, in: Proceedings of the American Control Conference, 2004. vol. 1, ISSN 0743-1619, 2004, pp. 239–244.

[16] Y. Fujisaki, Y. Oishi, R. Tempo, Randomized and deterministic algorithms for stabilization with fixed order controllers, in: Proceedings of the American Control Conference, vol. 2, ISSN 0743-1619, pp. 1214–1219.

[17] Y. Fujisaki, F. Dabbene, R. Tempo, Probabilistic robust design of LPV control systems, in: Proceedings of the 40th IEEE Conference on Decision and Control, 2001. vol. 2, 2001, pp. 2019–2024. http://dx.doi.org/10.1109/.2001.981207.

[18] O.J. Rojas, G.C. Goodwin, M.M. Serón, A. Feuer, An SVD based strategy for receding horizon control of input constrained linear systems, Internat. J. Robust Nonlinear Control (ISSN: 1099-1239) 14 (13–14) (2004) 1207–1226.

[19] M. Vukpbratovic, B. Boravac, Zero-moment point—thirty five years of its life, Int. J. Humanoid Rob. 01 (01) (2004) 157–173.

[20] A. Dutta, Design and certification of industrial predictive controllers (Ph.D. thesis), Ghent University, 2014.

[21] D. Clarke, C. Mohtadi, P. Tuffs, Generalized predictive control—Part I. The basic algorithm, Automatica (ISSN: 0005-1098) 23 (2) (1987) 137–148.

[22] M. Vukobratović, Legged Locomotion Robots and Anthropomorphic Mechanisms, Mihailo Pupin Institute, 1975.

[23] S. Kajita, F. Kanehiro, K. Kaneko, K. Fujiwara, K. Harada, K. Yokoi, H. Hirukawa, Biped walking pattern generation by using preview control of zero-moment point, in: Proceedings. ICRA'03. IEEE International Conference on, Robotics and Automation, vol. 2, ISSN 1050-4729, 2003, pp. 1620–1626.

[24] C. Moler, Numerical Computing with MATLAB, SIAM, Philadelphia, 2004, Print edition (Chapter 10).

[25] J.A. Castano, A. Hernandez, Z. Li, C. Zhou, N.G. Tsagarikis, D. Caldwell, R.D. Keyser, Implementation of robust EPSAC on dynamic walking of COMAN humanoid, in: 19th World Congress The International Federation of Automatic Control Cape Town, South Africa, August 24–29.

[26] H. Chen, F. Allgöwer, A quasi-infinite horizon nonlinear model predictive control scheme with guaranteed stability, Automatica (ISSN: 0005-1098) 34 (10) (1998) 1205–1217. http://dx.doi.org/10.1016/S0005-1098(98)00073-9.

[27] A. Bagheri, B. Miripour-Fard, Implementation of the model predictive control for on-line trajectory planning of a walking robot subjected to external disturbances, in: International Symposium in Innovations in Intelligent Systems and Applications, INISTA, 2011, pp. 590–594.

[28] J. Urata, K. Nshiwaki, Y. Nakanishi, K. Okada, S. Kagami, M. Inaba, Online decision of foot placement using singular LQ preview regulation, in: 11th IEEE-RAS International Conference on Humanoid Robots, Humanoids, ISSN 2164-0572, 2011, pp. 13–18.

[29] K. Harada, S. Kajita, K. Kaneko, H. Hirukawa, An analytical method on real-time gait planning for a humanoid robot, in: 2004 4th IEEE/RAS International Conference on Humanoid Robots, vol. 2, 2004, pp. 640–655. http://dx.doi.org/10.1109/ICHR.2004.1442676.

[30] B. Vanderborght, Dynamic Stabilisation of the Biped Lucy Powered by Actuators with Control stiffness, Springer, 2010.

[31] Zhibin Li, N.G. Tsagarikis, D. Caldwell, Walking pattern generation for a humanoid robot with compliant joints, Auton. Robots (ISSN: 0929-5593) 35 (1) (2013) 1–14.

[32] N.G. Tsagarakis, S. Morfey, G. Medrano Cerda, L. Zhibin, D.G. Caldwell, Compliant humanoid coman: Optimal joint stiffness tuning for modal frequency control, in: 2013 IEEE International Conference on Robotics and Automation, ICRA, ISSN 1050-4729, 2013, pp. 673–678.

Juan Alejandro Castano received his Bachelor's degree in Electronic Engineering in 2009 from Javeriana University, Colombia, and M.Sc. degree in Electronic Engineering in 2010 from Javeriana University, Colombia. He is currently a Ph.D. candidate with University of Genoa and Italian Institute of Technology. His research interests include dynamic walking control of humanoid robots and robust control.

Andres Hernandez received the bachelor degree in Electronic Engineering in 2007 and the M.Sc. degree in Control Engineering in 2011 from University of Ibague, Colombia, the last in lateral agreement with Ghent University, Belgium. He is currently Ph.D. researcher associated to the department of Electrical energy, Systems and Automation, Ghent University, Belgium. His main research interests are in systems modelling and identification, embedded optimization and model predictive control.

Zhibin Li graduated from the Harbin Institute of Technology (HIT) with the excellent graduate award in 2007 and obtained the Ph.D. degree at the Italian Institute of Technology (IIT) in 2012. He is currently a senior postdoctoral researcher in the Department of Advanced Robotics, IIT. His general research interest is dynamic motion control of robots, and his current work involves dynamic walking/balancing, push recovery control of legged robots, and admittance/impedance control of compliant actuators.

Nikos G. Tsagarakis received his D.Eng. degree in Electrical and Computer Science Engineering in 1995 from the Polytechnic School of Aristotle University, Greece, an M.Sc. degree in Control Engineering in 1997 and in 2000 a Ph.D. in Robotics from the University of Salford, UK. He is now Tenured Senior Scientist at IIT with overall responsibility for Humanoid design and Human Centred Mechatronics development. He is an author or co-author of over 250 papers in research journals and at international conferences and holds 14 patents. He is Technical Editor of IEEE/ASME Transactions in Mechatronics and on the Editorial Board of IEEE Robotics and Automation Letters and has been in the Program Committee of over 60 international conferences.

Darwin G. Caldwell is a Director at the Italian Institute of Technology, and a Honorary Professor at the Universities of Sheffield, Bangor, Tianjin, and Kings College London. His research interests include innovative actuators, humanoid and quadruped robotics and locomotion, haptics, exoskeletons, dexterous manipulators, rehabilitation and surgical robotics. He is the author or co-author almost 400 academic papers, and 15 patents.

Robin De Keyser graduated with a M.Sc. degree in Electro-Mechanical Engineering and obtained a Ph.D. degree in Control Engineering. He is currently full professor of Control Engineering at the Faculty of Engineering and Architecture, Ghent University, Belgium. His teaching and research activities are in model predictive control, auto-tuning and adaptive control, modelling and simulation, system identification, computer aided control systems design, signal processing, neuro-fuzzy and self-learning control. The research is application-driven, with many pilot implementations in technical and non-technical systems, amongst others mechatronic, energy, semiconductor, power electronics, chemical, food, steel, marine, logistics and biomedical engineering.

He is author/co-author of over 400 publications in journals, books, conference proceedings. Being one of the pioneers who produced the original concepts of predictive control during the 1980s, he developed and implemented the in-house EPSAC predictive control strategy and is mentioned as inventor in patents concerning industrial applications of this method.